Japanese Journal of Applied Physics

REGULAR PAPER

$BaTiO_3$-based composites provide new opportunities enabled by the cold sintering process

To cite this article: Toshiki Okazaki *et al* 2023 *Jpn. J. Appl. Phys.* **62** SM1030

Japanese Journal of Applied Physics **62**, SM1030 (2023) **REGULAR PAPER**
https://doi.org/**10.35848/1347-4065/acf478**

$BaTiO_3$-based composites provide new opportunities enabled by the cold sintering process

Toshiki Okazaki[1,2], Takao Sada[2], Kosuke Tsuji[3], Yoshihiro Fujioka[2], and Clive A. Randall[1*]

[1]*Materials Research Institute and Department of Materials Science and Engineering, The Pennsylvania State University, University Park, PA 16802, United States of America*
[2]*Kirishima R&D Center, KYOCERA Corporation, 1450-1 Kokubukamiogawa, Kirishima, Kagoshima, 899-4316, Japan*
[3]*Keihanna Research Center, KYOCERA Corporation, 3-5-3 Hikaridai, Seika-cho, Soraku-gun, Kyoto, 619-0237, Japan*

[*]E-mail: car4@psu.edu

Received August 17, 2023; revised August 25, 2023; accepted August 28, 2023; published online September 22, 2023

This paper reviews the synthesis of $BaTiO_3$-based ceramic and composites through the cold sintering process. Cold sintering is a densification process that works with a low-temperature mechanism known as pressure solution creep. This provides several opportunities to fabricate $BaTiO_3$ into new composite structures that could provide important advanced dielectric properties. Here we revisit the challenges of densifying a material such as $BaTiO_3$ that has incongruent dissolution. We consider the issues of surface chemistry, selection of transient flux, core–shell designs in $BaTiO_3$, co-sintering with polymers in the grain boundaries and the technical challenges associated with incorporating all these ideas into tape casting steps for future fabrication of multilayer device structures.

1. Introduction

Cold sintering is a low-temperature sintering process for sintering ceramics enabled by a sequence of mechanisms under a chemomechanical process collectively known as pressure solution creep and includes the interconnected kinetics controlling dissolution, mass transport and precipitation.[1–4)] The low temperatures and sufficient kinetics for densification can be activated with applied uniaxial pressures, moderate temperatures and an appropriate transient liquid phase. Cold sintering has enabled the fabrication of many dense ceramics at low temperatures (below 350 °C).[5–7)] Specifically, this technique has already been applied for some functional materials such as $BaTiO_3$,[8–10)] ZnO,[11,12)] $(K,Na)NbO_3$[13)] and $Li_{0.5}Al_{0.5}Ge_{1.5}(PO_4)_3$.[14,15)] $BaTiO_3$ is one of the most important electroceramic materials because of its dielectric properties and it is mainly used in multilayer ceramic capacitors.[16–18)] The need for more high-performance dielectrics is increasing because of advanced electrical systems such as electric vehicles and data transport and storage devices. This means that future capacitor designs need higher voltage operations at higher temperatures but also a high capacitive volumetric efficiency.[19–21)] This can be accomplished with reduced non-linear permittivity through suppression of voltage saturation, and coupled with higher degradation resistance would be a great technological advancement for these important materials.

2. Experimental methods

As this is largely a review, we do not cover all the aspects of the experiments and redirect readers to the original papers when appropriate. However, new data on tape casting aspects are covered here and to aid the reader. We therefore point to the important processing methodologies not previously discussed. In this part of the work the basic $BaTiO_3$ nanopowders synthesized by the typical oxalate method were used. The as-received $BaTiO_3$ nanopowder was calcined at 700 °C for 60 min to completely remove organic residues and carbonates.

Cold sintering was performed with 0.75 g of $BaTiO_3$ nanopowder and 0.11 g of $Ba(OH)_2{\cdot}8H_2O$ solid powder used as a transient liquid phase. Before sintering, these powders were ground and mixed homogeneously using a mortar and pestle. The mixture was loaded into a 12.7 mm diameter die and placed under uniaxial pressure of 350 MPa. The cold sintering process comprises two steps: pre-heating and cold sintering. In the pre-heating step the mixture was held at 80 °C for 30 min, a temperature close to the mp of $Ba(OH)_2{\cdot}8H_2O$(78 °C),[22)] using both a heater jacket and a press equipped with hot plates to melt flux and heat homogeneously. The second step of the cold sintering involves heating the mixture to 225 °C for 90 min under a pressure of 350 MPa. After the required heating time, the pressure was immediately released and the mixture cooled down to RT. The $BaTiO_3$ samples fabricated by this cold sintering process were dried in an oven at 120 °C overnight. The tape cast slurries were prepared from $BaTiO_3$ powder, $Ba(OH)_2{\cdot}8H_2O$ and polypropylene carbonate (QPAC 40, Empower Materials, New Castle, DE, USA). This slurry was prepared in a solvent of methyl ethyl ketone mixed by ball milling for 24 h. After removal of air bubbles using a slow rotating roller for 1 h, slurries were cast on a Mylar film with a doctor blade moving with a constant casting rate. The tape was dried and cut into 1.5 in (38.1 mm) squares. Then stacked with 22 layers (without any inner electrodes) and laminated under 45 MPa for 20 min at 75 °C. After lamination, the stacked tape was punched out into 0.5 in (12.7 mm) diameter circles. Binder burnout was conducted at 175 °C for 8 h in dry N_2. Cold sintering was attempted at 300 °C for 120 min under 350 MPa.

3. Results and discussion

A challenge with $BaTiO_3$ is the selection of a transient phase that must drive the dissolution and reprecipitation that underpin the processes, as represented in the schematic diagram in Fig. 1(a). $BaTiO_3$ is a compound that has a few surface chemistry details that must be carefully considered in the cold sintering process. Initially water was used in the transient phase when attempting cold sintering of $BaTiO_3$. Two major issues were encountered involving incongruent dissolution and the formation of $BaCO_3$ on the particle surfaces. Figure 1(b) shows the fundamental challenge with

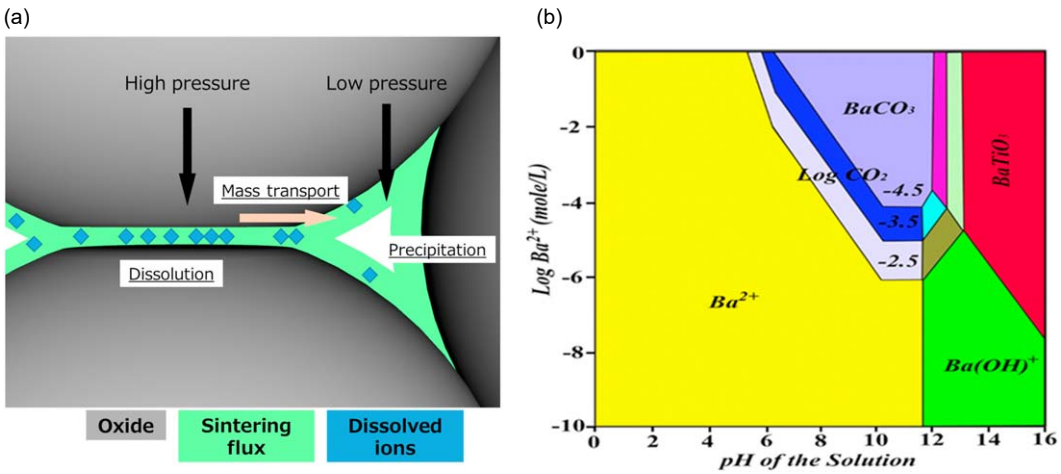

Fig. 1. (a) Representation of the pressure solution mechanism and interaction of the chemomechanical mechanism at particle-to-particle contacts under the applied pressure. (b) Ideal solubility phase diagram for $BaTiO_3$–H_2O–CO_2 as a function of pH.

the Ba^{2+} ion as a function of pH, being easily soluble to high concentrations; Ti^{4+}, irrespective of the pH, has a relatively very low solubility.[23–26)] The particle surfaces then become depleted in Ba ions, and the perovskite structure is broken down to an amorphous Ti surface layer. In cold sintering, dissolution would ideally be stoichiometric, and having the particle surface remain crystalline permits precipitation directly onto the crystallized surface by epitaxial growth when the transient phase is saturated with a stoichiometric balance of solute. Diffusion of Ba^{2+} ions into water occurs at low pH to high concentrations and the formation of $BaCO_3$ is favored at higher pH. This limits the dielectric properties despite permitting partial densification of the particles. A secondary heat treatment, namely heating the ceramic to above 800 °C, refines the grain boundaries and thereby recovers high-permittivity $BaTiO_3$ ceramics, allowing dense ceramics to be obtained. The cold sintered permittivity of ~70 increases to above 1600 after secondary heat treatment. The secondary temperature used is still much lower than the sintering temperature (1200 °C) for densifying $BaTiO_3$ under conventional methods. Others have confirmed our initial results and also identified the solution for applying the secondary heat treatment.[27,28)]

As we can see from Fig. 1(b), at high pH there are limits to the formation of $BaCO_3$ and there is also suppression of the incongruent dissolution of $BaTiO_3$. Tsuji et al. used a highly alkaline NaOH–KOH transient phase and found this to be very successful in both densifying the $BaTiO_3$ under the cold sintering process at 300 °C and giving high dielectric properties – all without having to resort to a secondary sintering process.[7)] This single-step process was accomplished in $BaTiO_3$ powders with particle sizes ranging from 20 nm up to 400 nm. The microstructure and associated dielectric properties of 95% densified $BaTiO_3$ cold sintered at 300 °C are shown in Fig. 2. The grain microstructure is highly faceted, and the dielectric permittivity is no longer limited by the $BaCO_3$ intergranular phase; the permittivity at RT is ~1500. However, there is a high dielectric loss of more than 5% at RT.

As an alternative transient flux for $Ba(OH)_2{\cdot}8H_2O$, a mixed powder strategy with nanosized (30 nm) TiO_2 was considered under a cold sintering process. The cold sintering temperatures were between 90 °C and 180 °C, and simultaneous densification and reactive synthesis of $BaTiO_3$ occurred. The non-$BaTiO_3$ phases were identified as a $BaCO_3$ phase and a residual TiO_2 phase. The reactivity necessary to form $BaTiO_3$ without a mineralizer is a noteworthy observation. Typically, these precursor reactants require water in a closed system and a hydrothermal process to form $BaTiO_3$. Here we note that the decomposition of $Ba(OH)_2{\cdot}8H_2O$ produces sufficient reactive water to drive $BaTiO_3$ synthesis. Second, it is likely that $BaCO_3$ formation is associated with removal of CO_2 from the atmosphere, as there was little or no carbonate in the initial powders. The dielectric properties after cold sintering are limited and very similar to the results obtained with the earlier water transient phase cases. So again, if we apply a secondary heat treatment at 900 °C for 3 h this removes the carbonate phase and establishes high dielectric properties, as shown in Fig. 3.

With the high reactivity shown from the $Ba(OH)_2{\cdot}8H_2O$ chemistry, Sada et al. directly explored it as a transient phase with $BaTiO_3$ powders.[8–10)] This led to high densification of between 94% and 98% of the $BaTiO_3$ at cold sintering temperatures between 150 °C and 280 °C. $Sr(OH)_2{\cdot}8H_2O$ was also found to be effective in the densification of both $BaTiO_3$ and $SrTiO_3$ powders under cold sintering.[29)] Figure 4(a) shows the phase diagram of the various $Ba(OH)_2{\cdot}H_2O$ systems. This diagram provides valuable insight into the respective dehydrated intermediate phases that occur under heating and a secondary phase is produced with the structural H_2O being released.[30,31)] In the case of $BaTiO_3$ sintered with the transient $Sr(OH)_2{\cdot}8H_2O$ phase this leads to the development of core–shell microstructure with the grains, as shown in Figs. 4(b) and 4(c). Transmission electron microscopy (TEM) and energy dispersive spectroscopy (EDS) reveal that the Ba and Ti ions dissolve into the flux and then undergo co-precipitation with epitaxial grain growth; shell formation from a mixture of Sr and Ba ions is inferred. This is consistent with the need to have a clean surface on which the precipitation of Ba, Sr, and Ti ions can ready occur, and therefore we also expect that the surface at high pH has undergone an incongruent dissolution process. There is some nonuniformity in the thicknesses of the shells in the grains relative to the applied pressure, and Sada et al.

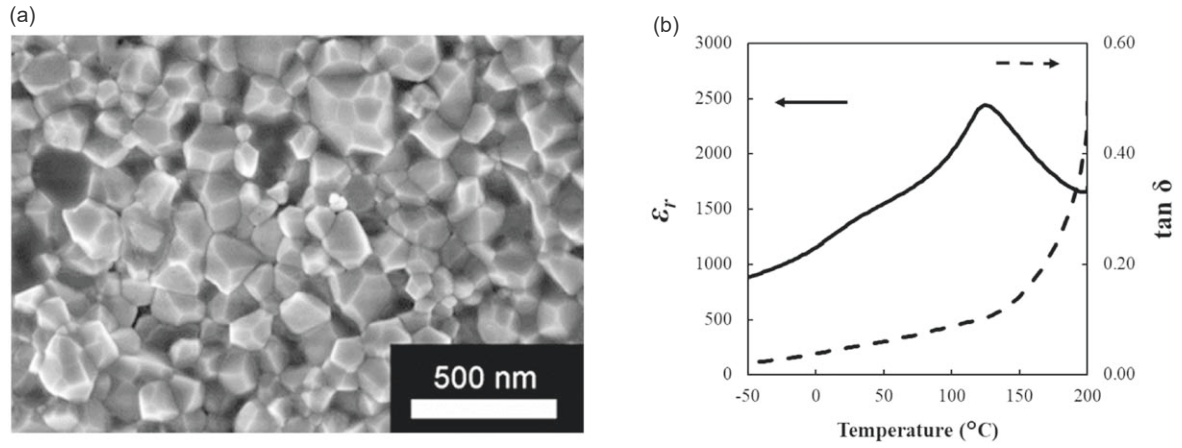

Fig. 2. (a) Microstructure of $BaTiO_3$ cold sintered with NaOH–KOH transient flux at 300 °C. (b) Associated dielectric permittivity the dielectric constant and dielectric loss over a temperature range from −50 °C to 200 °C.

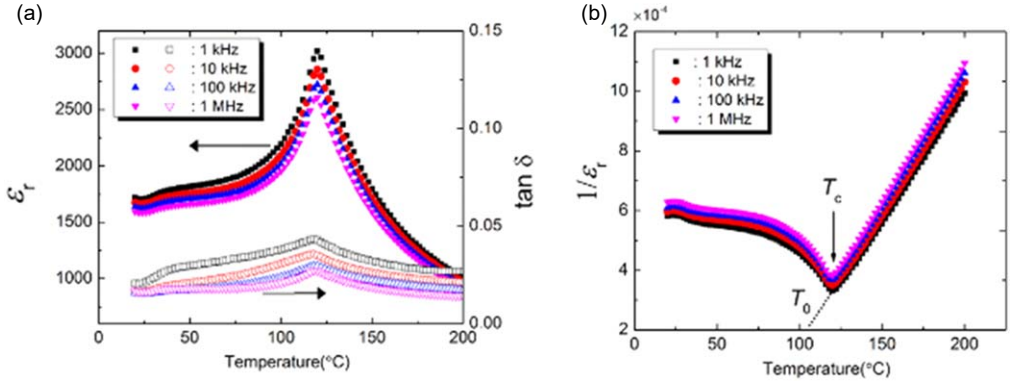

Fig. 3. (a) Temperature dependence of the dielectric properties. (b) Curie–Weiss plot for the 900 °C secondary heat treatment following reactive cold sintering with $Ba(OH)_2{\cdot}8H_2O$ and TiO_2 in an open system.

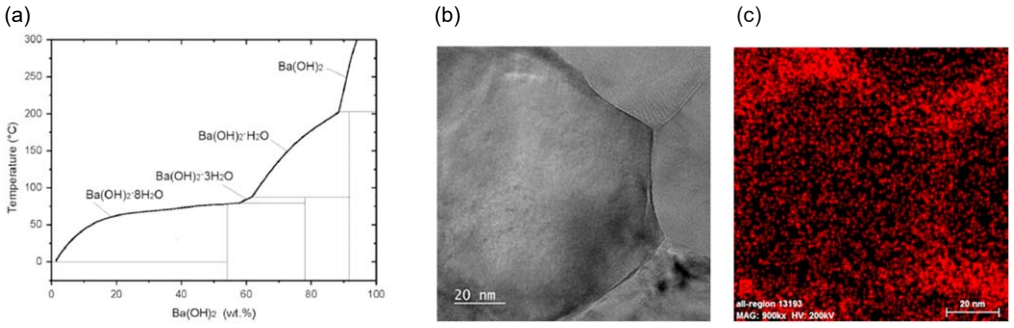

Fig. 4. (a) Phase diagram of the barium hydroxide–water system, redrawn from Kenisarin et al.[30] and using the data of Michaud.[31] (b), (c) A TEM microstructural image and the corresponding EDS data showing a core–shell microstructure.[29]

rationalized this within the pressure solution creep mechanism.[29]

With lower temperatures now possible for the densification of $BaTiO_3$, this opened the possibility of co-sintering organics such as polymers and surfactants into the grain boundaries of $BaTiO_3$ under cold sintering. The importance of this new type of dielectric composite is that it can overcome many of the inherent weaknesses of present day $BaTiO_3$ dielectrics in high-field operation. One of these weaknesses is the voltage saturation phenomenon, in which the permittivity is lowered under high electric field operation. Another weakness under high fields is the migration of oxygen vacancies, leading to time-dependent degradation of resistance of the insulation: a highly resistive polymer with low dielectric permittivity undergoes nanoscale integration into the grain boundaries between the high-permittivity $BaTiO_3$ grains. Partitioning of the electric fields with respect to the relative dielectric permittivity of each material as needed to have a continuous dielectric displacement field; this reduces the field strength in the grains and leads to strong field localization in the polymer grain boundaries. Thereby, the local fields are dramatically changed and the overall dielectric performance in the composite is enhanced.

This concept was first explored by Sada et al. for a number of polymers including the high-temperature thermoplastics polytetrafluorethylene (PTFE) and poly(*p*-phenylene oxide) (PPO). It was found that these materials could be sintered at low temperatures to an overall high density of ∼94% to 98%

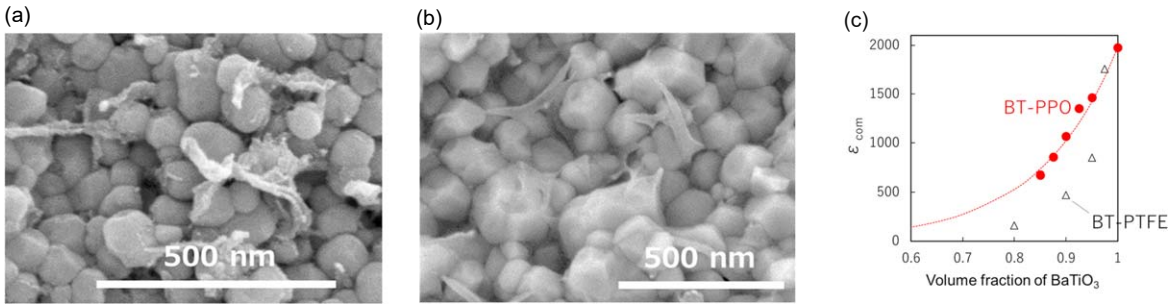

Fig. 5. SEM images of (a) $BaTiO_3$-PTFE(BT-PTFE) nanocomposite with 7.5 vol% PTFE and (b) $BaTiO_3$-PPO (BT-PPO) nanocomposite with 7.5 vol% PPO. (c) The RT dielectric constant of BT-PPO and BT-PTFE nanocomposite, with the dotted line being the estimated dielectric constant from the mixing law with homogeneous dispersion.

in the composites.[9,10] It was found that grafting of long PPO polymer molecules to the surfaces of the $BaTiO_3$ (100 nm particles) was the most effective way to maximize dispersion, relative to the dispersion of PTFE particles, as shown in Figs. 5(a) and 5(b). The better dispersion of polymer particles causes a higher dielectric constant, as shown as Fig. 6(c). Recently, Nunokawa et al. showed that with better mixing and dispersion of finer PTFE particles, $BaTiO_3$ PTFE composites with similar properties to the PPO composites could be realized.[32] The uniformity of the polymer is extremely important for obtaining a higher breakdown strength and time-dependent degradation resistance properties: like all mechanical or electric breakdown phenomena the fields can always find the weak points and therefore control the breakdown strength.

With several polymer strategies having now been demonstrated for the co-sintering of $BaTiO_3$ composites with the transient phase $Ba(OH)_2{\cdot}8H_2O$ we next look at the ability to add the $BaTiO_3$ and $Ba(OH)_2{\cdot}8H_2O$ to a low-temperature binder system that can be cast and undergo binder burnout without dehydration or reaction that would limit the subsequent densification. The ability to cold sinter multilayers with a tape cast formulation, using the binder polyalkylene carbonate (QPAC) was previously demonstrated; this then becomes the natural choice for this initial investigation into multilayer processing.[33–35] This is a very attractive candidate as it can be removed under a thermal decomposition process at temperatures as low as 120 °C in air and nitrogen atmospheres. Under the debinding decomposition process QPAC produces CO_2 and H_2O that evolve within the particle mixture of $BaTiO_3$ and the transient phase. Before considering this stage it is important to note that there is no interaction of the binder system with a strong base such as $Ba(OH)_2{\cdot}8H_2O$. Such reactions could decompose the polymer and the hydroxide phase, limiting the casting, forming and ultimately the cold sintering processes.

Using X-ray diffraction, we can determine any significant phase changes and find the relative percentage of these phases through the various processes involved in the tape casting; in particular, the monitoring of $BaCO_3$ formation becomes important. In the milling of powders, milling/mixing with the polymers and solvents and tape casting there was no indication of an increase in the $BaCO_3$ content. The first indication of such an increase comes with the lamination condition, as shown in Fig. 6(a). The initial lamination condition was at a temperature of 75 °C. As noted in Fig. 4(a), this is close to the mp of $Ba(OH)_2{\cdot}8H_2O$, and the hydroxide is then activated to react easily with organics and form a carbonate with up to 25 wt% $BaCO_3$. To prevent reaction between the hydroxide and the organic binder and its constituents, RT uniaxial lamination was performed under 56 MPa for 5 min, avoiding the high-temperature lamination process and the potential carbonate reactions. Uniaxial pressures between 56 MPa and 426 MPa at RT enabled lamination without carbonate formation, as shown in Fig. 6(b).

With the binder burnout process occurring at 175 °C for 8 h in dry N_2, $Ba(OH)_2{\cdot}8H_2O$ and the other dehydrated $Ba(OH)_2{\cdot}xH_2O$ compounds mainly react with CO_2 derived from binder decomposition and form a deleterious $BaCO_3$ carbonate phase that limits densification and high dielectric properties without using the aforementioned secondary heat

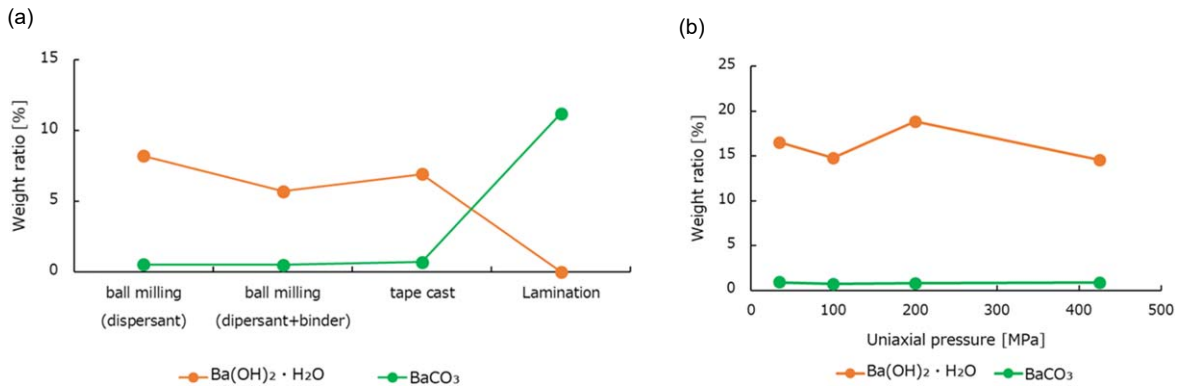

Fig. 6. (a) The change of $BaCO_3$ with respect to the process using polyalkylene carbonate tapes prior to cold sintering. (b) The change of $BaCO_3$ with different applied uniaxial pressures.

treatments to remove the carbonates. Various strategies have been considered to prevent or suppress the formation of carbonates, including the use of lower levels of hydrated $Ba(OH)_2{\cdot}xH_2O$ ($x = 3$, 2, 1, and 0). At this stage using this low-temperature QPAC binder system we have not yet not succeeded in preventing substantial $BaCO_3$ formation without deactivating the transient phase, and thereby limiting the cold sintering densification. This now becomes the next challenge: to finding a processing route to fabricate cold sintered multilayer composites. This may need a new binder polymer strategy, or a new formation process such as electrophoretic deposition, or an alternative electrospray technology to lay down the multilayer structures. We are not considering small capacitors in this strategy, rather larger ones than the conventional fired multilayers we are using today. There is a need for the larger capacitor types for future power electronic applications.

4. Summary and conclusions

We have considered the recent evolution of cold sintering of $BaTiO_3$ ceramics and its composites to form high-performance materials at extremely low temperatures. Various transient phases have been demonstrated and processes adjusted to enable high-performance dielectric properties. In the first-generation studies, transient phases used water and acidic pH solutions, but these are limited by the incongruent dissolution of Ba^{2+} ions and the formation of intergranular carbonate phases. A secondary thermal treatment removed the carbonates, continually evolving the microstructure and the properties. These secondary temperatures are still much lower than the typical conventional sintering temperatures for $BaTiO_3$. The second-generation transient phases for $BaTiO_3$ used NaOH–KOH to develop extremely high-performing dielectrics at temperatures of ~300 °C in a single-step process. Third-generation methods used $Ba(OH)_2{\cdot}8H_2O$, and related fluxes for cold sintering in a single step at temperatures between 150 °C and 280 °C. This could densify pure $BaTiO_3$ and core–shell structures with (Ba, Sr)TiO_3 shell compositions. At these lower temperatures novel polymer–$BaTiO_3$ composites with high-temperature thermoplastics and different surfactants have enabled integration of polymeric grain boundaries within the materials. These composites are enabling a new strategy for manipulating the high-field properties of the $BaTiO_3$ and related materials using local field distributions. Properties such as resistivity, non-linear dielectric properties, dielectric breakdown and time-dependent dielectric breakdown are all improved within these composites. Finally, we outline the next technical challenge of developing a multilayer process for composite $BaTiO_3$ structures. The need to balance the binder removal process without limiting the dehydration of the transition phases such as $Ba(OH)_2{\cdot}8H_2O$ that couples to the cold sintering process of pressure solution creep. In addition, the polymer must not decompose and the CO_2 product reactively forms a carbonate on the $BaTiO_3$ surface.

Acknowledgments

TO would like to thank the Kyocera Corporation for the visiting scientist fellowship that enabled the scientific studies at the Pennsylvania State University. We would also thank the staff from the Materials Characterizing Laboratory in The Materials Research Institute. CAR would also like to thank the National Science Foundation NSF_FMSG (2134643) program and DMR-2202525 for partial support of this work. We would also like to thanks Empower Materials for the supply of QPAC binder.

1) X. Zhang and C. J. Spiers, Geochim. Cosmochim. Acta **69**, 5681 (2005).
2) D. W. Durney, Nature **235**, 315 (1972).
3) C. J. Spiers, P. M. T. M. Schutjens, R. H. Brzesowsky, C. J. Peach, J. L. Liezenberg, and H. J. Zwart, Geol. Soc. Spec. Publ. **54**, 215 (1990).
4) A. M. H. Pluymakers and C. J. Spiers, Geol. Soc. Spec. Publ. **409**, 107 (2015).
5) H. Guo, J. Guo, A. Baker, K. Shiratsuyu, and C. A. Randall, ACS Appl. Mater. Interfaces **8**, 20909 (2016).
6) J. Guo, H. Guo, A. L. Baker, M. T. Lanagan, E. R. Kupp, G. L. Messing, and C. A. Randall, Angew. Chem. **128**, 11629 (2016).
7) K. Tsuji, A. Ndayishimiye, S. Lowum, R. Floyd, K. Wang, M. Wetherington, J.-P. Maria, and C. A. Randall, J. Eur. Ceram. Soc. **40**, 1280 (2020).
8) T. Sada, K. Tsuji, A. Ndayishimiye, Z. Fan, Y. Fujioka, and C. A. Randall, J. Eur. Ceram. Soc. **41**, 409 (2021).
9) T. Sada, K. Tsuji, A. Ndayishimiye, Z. Fan, Y. Fujioka, and C. A. Randall, J. Appl. Phys. **128**, 084103 (2020).
10) T. Sada, K. Tsuji, A. Ndayishimiye, Z. Fan, Y. Fujioka, and C. A. Randall, Adv. Mater. Interfaces **8**, 2100963 (2021).
11) S. Funahashi, J. Guo, H. Guo, K. Wang, A. Baker, K. Shiratsuyu, and C. A. Randall, J. Am. Ceram. **100**, 546 (2017).
12) X. Kang, R. Floyd, S. Lowum, M. Cabral, E. Dickey, and J.-P. Maria, J. Am. Ceram. **102**, 4459 (2019).
13) K. Tsuji, Z. Fan, S. H. Bang, S. Dursun, S. T. McKinstry, and C. A. Randall, J. Eur. Ceram. Soc. **42**, 105 (2022).
14) S. Berbano, J. Guo, H. Guo, M. T. Lanagan, and C. A. Randall, J. Am. Ceram. **100**, 2123 (2017).
15) K. Takashima, Y. Iwazaki, and C. A. Randall, Jpn. J. Appl. Phys. **60**, 126505 (2021).
16) H. Kishi, Y. Mizuno, and H. Chazono, J. Appl. Phys. **42**, 1 (2003).
17) C. Pithan, D. Hennings, and R. Waser, Int. J. Appl. Ceram. Technol. **2**, 1 (2005).
18) A. J. Bell, J. Eur. Ceram. Soc. **28**, 1307 (2008).
19) H. Palneedi, M. Peddigari, G.-T. Hwang, D.-Y. Jeong, and J. Ryu, Adv. Funct. Mater. **28**, 1803665 (2018).
20) J. Watson and G. Castro, J. Mater. Sci.: Mater. Electron. **26**, 9226 (2015).
21) Z. Yao, Z. Song, H. Hao, Z. Yu, M. Cao, S. Zhang, M. T. Lanagan, and H. Liu, Adv. Mater. **29**, 1601727 (2017).
22) I. A. Tahiri, Matiullah, and M. S. Subhani, Radiat. Meas. **37**, 205 (2003).
23) A. Neubrand, R. Lindner, and P. Hoffmann, J. Am. Ceram. Soc. **83**, 860 (2004).
24) K. Osseo-Asare, F. J. Arriagada, and J. H. Adair, *Ceramic Transaction, Ceramic Powder Science II A* (American Ceramic Society, Westerville, OH, 1988) Vol. 1, p. 47.
25) P. Bendale, S. Venigalla, J. R. Ambrose, E. D. Verink, and J. H. Adair, J. Am. Ceram. Soc. **76**, 2619 (1993).
26) M. M. Lencka and R. E. Riman, Chem. Mater. **5**, 61 (1993).
27) H. Guo, A. Baker, J. Guo, and C. A. Randall, ACS Nano **10**, 10606 (2016).
28) J. P. Ma, X. M. Chen, W. Q. Ouyang, J. Wang, H. Li, and J. L. Fang, Ceram. Int. **44**, 4436 (2018).
29) T. Sada, Z. Fan, A. Ndayishimiye, K. Tsuji, A. Y. Fujioka, and C. A. Randall, J. Am. Ceram. Soc. **104**, 96 (2020).
30) M. Kenisarin and K. Mahkamov, Sol. Energy Mater. Sol. Cells **145**, 255 (2016).
31) M. Michaud, CR Acad. Sci. **262**, 1143 (1966).
32) T. Nunokawa, K. Takashima, K. Mizuno, and C. A. Randall, Jpn. J. Appl. Phys. **62**, 071003 (2023).
33) J. Guo, X. Zhao, T. Herisson De Beauvoir, J.-H. Seo, S. S. Berbano, A. L. Baker, C. Azina, and C. A. Randall, Adv. Funct. Mater. **28**, 1801724 (2018).
34) T. H. de Beauvoir, S. Dursun, L. Gao, and C. A. Randall, ACS Appl. Electron. Mater. **1**, 1198 (2019).
35) H. Yang, W. Bao, Z. Lu, L. Li, H. Ji, Y. Huang, F. Xu, G. Wang, and D. Wang, J. Mater. Res. **36**, 1285 (2021).

